Published in final edited form as:
J Mol Med (Berl). 2011 March ; 89(3): 263–277. doi:10.1007/s00109-010-0700-8.

Morphogenesis and maintenance of the 3D-thymic medulla and prevention of nude skin phenotype require FoxN1 in pre- and post-natal K14 epithelium

Jianfei Guo[1,2], **Moshiur Rahman**[1,2], **Lili Cheng**[1,2], **Shuangmin Zhang**[1], **Amy Tvinnereim**[1], and **Dong-Ming Su**[1,2,*]

[1]Department of Biomedical Research, University of Texas Health Science Center at Tyler, Tyler, TX, 75708, USA.

[2]Department of Molecular Biology and Immunology, University of North Texas Health Science Center at Fort Worth, Fort Worth, TX, 76107, USA.

Abstract

Expansion of thymic epithelial cysts represents disruption of an organized three-dimensional (3D) thymic epithelial cell (TEC) meshwork, which is crucial for T-lymphocyte development. Although the *FoxN1*-null mutant develops a rudimentary 2D-cystic thymus, 2D-thymic cyst-lining resulting from a dGUO culture was reported to be FoxN1-independent, thus, it is unclear whether loss of FoxN1 facilitates cyst formation, and whether FoxN1 regulates the morphogenesis and maintenance of the 3D-thymic microstructure. Using the *loxP*-floxed-*FoxN1* mouse model, we demonstrated that specific deletion of *FoxN1* in Keratin (K)-14 promoter-driven TECs induced the loss of 3D-thymic medullary structure by producing a large number of morphologic pulmonary alveolar-like 2D-epithelial cysts, which increased with age. The cyst-lining was positive for differential polarized keratins and had strong Claudin-3,4, but reduced MHC-II, expression. However, an increased % of Claudin-3,4$^+$ TECs, which are presumptive precursors of UEA-1$^+$ and Aire$^+$ mature medullary TECs, failed to promote the development of these mature descendants. Meanwhile, the K14Cre-mediated *FoxN1* deletion alone was sufficient to induce a complete hair follicle defect, causing a nude phenotype in the skin, but was not sufficient to cause a complete loss of the thymus. All these changes to occur require deletion of *FoxN1* in both prenatal (Cre-recombinase from parents during fertilization) and postnatal (Cre-recombinase from offspring themselves after fertilization) life. These findings provide new insights into FoxN1 regulation of 3D-thymic epithelial morphogenesis and maintenance, the distinct impacts of FoxN1 in the K14 epithelial subset of the thymus and skin, and its postnatal requirement.

Keywords

K14-Epithelium; *FoxN1* gene; thymic cysts; nude skin, *loxP*-Cre recombination system

Introduction

The functional thymus, composed primarily of an integrated and organized three-dimensional (3D) meshwork of thymic epithelial cells (TECs), provides a unique microenvironment to foster developing T-lymphocytes, mainly αβ T-cell receptor (TCR)-

*Corresponding author: Department of Molecular Biology and Immunology, University of North Texas Health Center at Fort Worth, Fort Worth, TX, 76107 USA. Tel. 1-817-735-5186, Fax: 1-817-735-0375, dong-ming.su@unthsc.edu .

Author Information The authors declare that they have no competing financial interests.

lineage T-cells. In the T-cell developmental pathway, lympho-hematopoietic progenitor/stem cells (LPCs) emigrate from the bone marrow to the 3D thymus, where the developing T-precursors, namely thymocytes, interact with TECs and other thymic stromal cells (TSCs), and undergo multiple processes including migration, proliferation, lineage-specification, differentiation, apoptosis, and TCR rearrangement to become functional T-cells. Mature T-cells containing a functionally competent TCR that is reactive to foreign antigens, but tolerant to self-antigens, emigrate to peripheral lymphoid tissues, where they mediate host immunity.

Unlike most other epithelial organs that are composed of polarized two-dimensional (2D) sheet-like epithelial cells with apical-lumen and basal-layer, the functional thymic epithelium is an organized 3D meshwork [1] developed by cross-talk with developing T-progenitors from a 2D-apico-basal stratified thymic anlage during organogenesis. In the mature thymus, the 3D-orientation of TECs largely contributes to the basis of thymic microenvironment, but the residual 2D-apico-basal structure can still be seen, persisting as an epithelial cystic cavity [2-4]. The number of these thymic cysts expands with age in wild type (WT) mice [4], under abnormal culture conditions, and when there is a reduction in lympho-stromal interactions [4,5], as well as in certain gene knockout, such as aly/aly [6] mice.

Based on anatomic, cell marker, and functional criteria, thymic epithelial regions can be divided into the cortex and medulla, which provide different microenvironments that are responsible for key stages in thymocyte development [7]. The thymic cortex primarily provides a microenvironment for the development of $CD4^{-}8^{-}$ double negative (DN) and $CD4^{+}8^{+}$ double positive (DP) thymocytes, and positive (in part negative) selection [8] of their TCRs to ensure reactivity and specificity to foreign antigens. The thymic medulla is mainly involved in the generation of central immune tolerance by providing a microenvironment for the negative selection and depletion of self-reactive T-cell clones during thymocyte development. Clonal deletion is largely achieved by intercellular self-antigen transfer [9]. These antigens are peripheral-tissue restricted antigens (TRAs) presented by medullary TECs (mTECs) and thymic dendritic cells in the medulla, where thymocytes encounter these ubiquitous antigens which are expressed in a “promiscuous” fashion. The expression of about 1/3 of TRAs in mTECs is primarily controlled by the *Aire* (autoimmune regulator) gene [10]. The thymic medulla begins to be formed at ~day-15 of fetal development (embryonic day-15, E15) in mice, and progressively increases in size, becoming well established by the third postnatal week [11]. A reduction in the size of the medulla can affect the efficiency of presenting TRAs [12], thus a poorly developed medulla may increase the incidence of autoimmune diseases.

Since TECs are similar to keratinocytes in the skin, immunofluorescent keratin (K) antibodies are widely used to identify thymic epithelial cells in the cortical and medullary regions [13]. Generally, $K8^{+}K5^{-}$ TECs are the predominant cortical TECs (cTECs) and $K8^{-}K5^{+}$ TECs are the predominant medullary TECs (mTECs), while $K8^{+}K5^{+}$ TECs are either immature TECs (precursors of cTECs or mTECs) in the fetal thymus [14] or TECs located at the cortico-medullary junction (CMJ) in the mature thymus. $K14^{+}$ TECs are the major pairing partners of $K5^{+}$ TECs, and both are basal keratins of stratified squamous epithelium. The human K14 (hK14) promoter can direct gene expression in the basal layer of mouse skin, esophagus, and tongue in a manner analogous to that of the endogenous K14 gene [15]. While the basal epithelium forms the epithelial progenitor cells, and the hK14 promoter exhibits activity in epithelial progenitor cells in the skin and mammary gland [15,16], these features are undetermined in the thymus.

An epithelial cell-autonomous gene forkhead box N1 (*FoxN1*) is required for thymic epithelial patterning and differentiation from the initial epithelial thymic anlage to a functional cTEC and mTEC meshwork during crosstalk with the lymphoid compartment. A null mutation in *FoxN1* [17,18] causes failure of TECs to differentiate, thereby halting development of the thymus at a rudimentary stage [17], resulting in an alymphoid 2D-cystic thymic rudiment and nude phenotype in both mouse (nude mouse) and human [19]. Recently, the abnormal culture (dGUO) condition-induced 2D-thymic cyst-lining was reported to be non-FoxN1-dependent [4], which makes it unclear whether the loss of FoxN1 promotes the formation and expansion of 2D-thymic cysts, and whether FoxN1 is required for morphogenesis and maintenance of the 3D-thymic microstructure. In addition, the mechanism by which *FoxN1* regulates keratin-type-specific promoter-driven epithelium in the thymus has not yet been addressed. To fill this gap we used a tissue-specific *FoxN1* mutant model – K14Cre-fx mouse model, generated by crossing a *loxP*-floxed-*FoxN1*-exons 5&6 (denoted as "fx") mouse [20] with a hK14-Cre transgenic mouse [21], to study keratin type-specific loss-of-function of *FoxN1* both during and after thymic organogenesis. This mouse model is neither equivalent to the 100% *FoxN1* gene mutant – nude mouse [17], nor the *FoxN1* partial/hypomorphic mutant – FoxN1Δ mouse [22]. It is a keratin14-specific novel *FoxN1* mutation. We found that progressive deletion of *FoxN1* exons 5&6 in K14 promoter-driven TECs in both prenatal and postnatal life (rather than in prenatal life alone) resulted in the formation of a large number of morphologic pulmonary alveolar-like cystic cavities that were Claudin-3&4 (Cld3,4) positive and expressed differential polarized keratins in the thymic medulla, and whole numbers were increased with age. Furthermore, the deterioration of the thymus from 3D to 2D reduced major histocompatibility complex class II (MHC-II) expression, which is a mature TEC marker, and decreased the number of UEA-1^+ and $Aire^+$ mature mTECs. Meanwhile, deletion of *FoxN1* in prenatal and postnatal life (rather than in prenatal life alone) solely in K14 promoter-driven epithelia was sufficient to induce a *FoxN1*-null nude phenotype in the skin, but did not induce athymia, which differs from the *FoxN1*-null nude thymic phenotype. This indicates that FoxN1 is potentially involved in the regulation of 3D-thymic epithelial morphogenesis and maintenance, and FoxN1 in K14-driven epithelial cells may have distinct roles/impacts in the thymus and skin.

Material and Methods

Mice and animal care, genotyping and determination of FoxN1 genomic DNA deletion

The $FoxN1^{flox}$ (fx) mice, in which exons 5 and 6 (DNA binding domain) of the *FoxN1* locus are flanked by two *loxP* sites, were generated in a C57BL/6/129Sv genetic background, as described previously [20] and donated to Jackson Lab (#012941). K14Cre-fx/fx and -fx/+ mice were generated by crossbreeding fx mice with Keratin-14 promoter-driven Cre-recombinase transgenic (K14Cre) mice [21], from the Jackson Laboratory (#004782). All young mice were genotyped by PCR with a set of three fx primers A, B and C (Fig. 1A) [20] and K14Cre primers (Supplemental Table S1). The ratio of Cre-mediated *loxP*-floxed *FoxN1* deletion in the skin was determined by PCR using genomic DNA with primers B and C shown in Figure 1A. Ages of the mice used are indicated in each figure legend. All animal experiments were in compliance with the protocols approved by the Institutional Animal Care and Use Committee of the University of Texas Health Science Center at Tyler, in accordance with guidelines of the National Institutes of Health, USA.

Analysis of gene expression with real-time RT-PCR

Total RNA from mouse skin and thymus was prepared and reverse transcribed with TRIzol and the SuperScriptIII cDNA kit (Invitrogen). Real-time PCR was performed by the TaqMan® method in a StepOnePlus thermocycler (Applied Biosystems). The *FoxN1* primers and probe for real-time RT-PCR (TaqMan® method) are listed in Supplemental

Table S1. The *Aire* primers and probe for real-time RT-PCR (TaqMan® method) were purchased from TaqMan® Gene Expression Assays (Cat# Mm00477461_ml, Applied Biosystems), and primers for the semi-quantitative RT-PCR are listed in Supplemental Table S1. Each sample was analyzed by duplicate PCR reactions, and normalized to 18s rRNA for real-time RT-PCR or GAPDH for semi-quantitative RT-PCR as the internal control. The results were analyzed by the relative quantification (RQ) of gene expression by the $\Delta\Delta C_T$ method calculated based on the Livak method by following the instructions from Applied Biosystems, setting the value for control cDNA as 1.0.

Histological and immunofluorescent (IF) analysis

For H&E staining, 5 μm-thick serial paraffin tissue sections were stained with hematoxylin and eosin (H&E). For immunofluorescent staining, 6 μm-thick serial cryosections were fixed in cold acetone, blocked with 10% donkey serum in TBS, and stained with optimized diluted dual primary antibodies, followed by optimized diluted fluorochrome-conjugated dual secondary antibodies. Primary antibodies include rabbit anti-FoxN1 (previously used, [20])/goat anti-FoxN1 (clone G20, Santa Cruz), rabbit anti-AIRE-1 (M-300, Santa Cruz) [23], rabbit anti-mouse K5 (Covance), rabbit anti-mouse Claudin-3,4 (Cld3,4, Invitrogen, #34-1700 and #36-4800), rat anti-mouse K8 (Troma-1 supernatant), rat anti-mouse MHC-Class-II (I-A/I-E, BioLegend), and biotinylated-anti-UEA-1 (Vector Labs). Secondary reagents include Cy3-donkey anti-rabbit IgG, Cy3-streptavidin, FITC-donkey anti-rat IgG (Jackson Immunoresearch Laboratories), and Alexa-Fluor-488-anti-rabbit IgG (Invitrogen). Antibody-stained immunofluorescent samples were mounted with anti-fading aqueous mounting medium and coverslipped. The slides were observed using Nikon Eclipse Ti-U and Carl Zeiss LSM 510 confocal fluorescent microscopes and the magnification of the objective lens is indicated in each figure.

Flow cytometry assay

For FACS analysis, thymocytes isolated with a cell-strainer were stained with fluorochrome-conjugated anti-CD4 and anti-CD8 (BioLegend), and TSCs or TECs isolated from the Collagenase-V/DNase-I-dissociated thymus [24] were stained with combinations of PE/Cy5-conjugated anti-mouse-CD45, FITC-conjugated UEA-1 (Vector Labs), and Cld3,4 (Invitrogen) plus APC-conjugated anti-Rat IgG (Jackson Immunoresearch Laboratories). Data were acquired with a dual-laser FACS Calibur system and analyzed using CellQuest and FlowJo software.

Statistics

The statistical significance between any two groups was analyzed by unpaired Student's *t*-test. If the F-test comparison of variance was less than 0.05 (i.e. nonparametric distribution), the unpaired *t*-test with Welch's correction was used. Differences were considered statistically significant at values of $p < 0.05$. All measures of variance are presented as SEMs.

Results

Keratin type-specific deletion of FoxN1 exon-5 & -6 mediated by K14Cre from parents and self, during and after fertilization, causes a nude skin phenotype

A schematic diagram of *loxP*-floxed *FoxN1* mice crossed to K14Cre mice, before (top) and after (bottom) K14Cre mediated excision of *FoxN1* exon-5 and -6 (denoted as "K14-ΔE5&6-deletion") is shown in Figure 1A. Unlike the $CreER^T$ transgene, the Cre transgene-mediated *loxP*-floxed-gene deletion occurs in germline cells and usually during fertilization *in utero* when the mother carries the Cre transgene. To determine whether paternal Cre is

also able to mediate K14-ΔE5&6-deletion, we performed two mating strategies: female K14Cre^{+} mice crossed with male K14Cre^{-} mice and female K14Cre^{-} mice crossed with male K14Cre^{+} mice. We found that the K14Cre-mediated *FoxN1* recombination occurred in offspring from both mating strategies (Table 1 and Supplemental Fig. S1), which corroborates previous reports in both K14Cre [25] and K5Cre [26] transgenic mice.

One of the typical phenotypes of the FoxN1-null mutation is nude skin resulting from a hair follicle developmental defect caused by a block in the differentiation of epithelial stem cells. Since the K14 promoter exhibits activity in epithelial stem cells, we asked whether the K14-ΔE5&6-deletion in germ cells in which the K14 promoter is active is sufficient to induce the FoxN1-null phenotype in the skin. As it turned out, the K14-ΔE5&6-deletion in the skin of the K14Cre-fx mice resulted in the failure of hair follicles to develop (Figs. 1B-F).

Interestingly, we found that the fx/fx homozygous mice with the K14-ΔE5&6-deletion (Fig. 1C, middle and right lanes of top panel) exhibited two different phenotypes in the skin. One was haired while the other was nude (Fig. 1B, left and middle mice). Given the K14Cre PCR results, we found that the haired-fx/fx mice with the K14Cre-mediated *FoxN1* ΔE5&6-deletion (haired-K14-ΔE5&6-deletion) were K14Cre transgenic negative (Fig. 1C, middle lane of bottom panel), while the nude-fx/fx mice with the K14Cre-mediated *FoxN1* ΔE5&6-deletion (nude-K14-ΔE5&6-deletion) contained the K14Cre transgene (Fig. 1C right lane of bottom panel). This implies that in the haired-K14-ΔE5&6-fx/fx mice, the ΔE5&6-deletion band is a history of *FoxN1*^{flox} recombination mediated by their parental K14Cre Tg during fertilization rather than themselves', because these mice do not have K14Cre Tg while they have K14Cre-mediated *FoxN1*-ΔE5&6-deletion. In addition, we found that the haired mice with K14-ΔE5&6-deletion had a normal thymus, while the nude mice with K14-ΔE5&6-deletion had a defective thymus. Therefore, *FoxN1* ΔE5&6-deletion occurs both during (Cre expression in the parents) and after (Cre expression in the offspring themselves) fertilization cause phenotypes, while the K14-ΔE5&6-deletion in prenatal development alone is not sufficient to induce the skin and thymic phenotypes. It may be the case that K14Cre-medicated ΔE5&6-deletion is not in 100% K14^{+} epithelial cells in early young age. That is why we did not find thymic cysts (Details are addressed in the following sections) in the thymus before two weeks old. However, as the existed K14Cre transgene continuously produces Cre recombinase in K14^{+} epithelial cells, thymic cysts keep being increased and phenotype becomes severe with age. This is the evidence that the deletion is either complete or sufficient enough in the adult mouse to the K14-ΔE5&6-deletion-related phenotypes. The levels of K14-ΔE5&6-deletion in genomic DNA (Fig. 1D) and *FoxN1* mRNA expression (Fig. 1E) in the skin of haired-fx/fx mice with the K14- ΔE5&6-deletion (deletion caused solely by parental Cre) were not significantly different from those of the K14Cre-expressing fx-heterozygous (K14Cre-fx/+) littermate controls. However, the skin of the nude-K14Cre-fx/fx mice, in which the K14-ΔE5&6 deletion is mediated by Cre from both the parents and offspring self, exhibited a significant increase in K14-ΔE5&6-deletion (Fig. 1D, triangles) with a corresponding significant decrease in *FoxN1* mRNA levels (Fig. 1E, triangles), compared to the heterozygous littermate controls.

In addition, we found the nude phenotype in nude-K14Cre-fx/fx mice to be identical to that reported in naturally occurring *FoxN1*-null nude mice [27,28], involving a hair follicle defect in the hair cortex (Fig. 1F, arrowhead in lower right panel) and degradation of the hair root under the skin surface (Fig. 1F, arrows in lower right panel), whereas the skin hair follicles in the haired-fx/fx mice with the K14-ΔE5&6-deletion exhibited normal hair development (Fig. 1F, middle panels), and were indistinguishable from heterozygous littermate controls (Fig. 1F, left panels). The results indicate that the K14-ΔE5&6-deletion, occurring in both prenatal and postnatal life rather than prenatal life alone, in K14-promoter-

driven epithelium can be sufficient to induce a hair follicle defect in development and causes a nude phenotype.

Nude-K14Cre-fx/fx mice have a developmental defect in the thymus that differs from FoxN1-null athymia

Moving our focus to the thymus, we found that haired-fx/fx mice with a K14-ΔE5&6-deletion generally had a normal thymus that was similar to the thymus in heterozygous littermate controls, but the nude-K14Cre-fx/fx mice had a defective thymus. Although the nude-K14Cre-fx/fx mice had a nude skin phenotype that is similar to the naturally occurring *FoxN1*-null mutant mice (Fig. 1), to our surprise, their thymus, while reduced in size, had not completely disappeared (Fig. 2A, right sample, and supplemental Fig. S2), which is quite different from the athymia (an alymphoid anlage) observed in the naturally occurring *FoxN1*-null mice. Furthermore, the profile of CD4 versus CD8 thymocyte subsets in the nude-K14Cre-fx/fx mice (Fig. 2B, third panel from left) was different from that of naturally occurring *FoxN1*-null nude mice [17] (Fig. 2B, rightmost panel).

In the nude-K14Cre-fx/fx thymi FoxN1 mRNA was significantly reduced (Supplemental Fig. S3A) and $FoxN1^+$ TECs (protein level) were also overtly reduced (Supplemental Fig. S3B, lower panels). A few $FoxN1^+$ nuclear staining spots were present in or overlapped with $K5^+$ but not in/with $K14^+$ TECs (Supplemental Fig. S3C). The absolute numbers of total thymocytes, $CD4^+8^+$ double positive (DP), $CD4^+$ single positive (SP), and $CD8^+$SP cells were all significantly decreased (Fig. 2C, left and right panels), but the proportions of those subsets did not change (Figs. 2B 1-3 panels from left, and C, middle panel). The thymoycte phenotype in the nude-K14Cre-fx/fx mice is reminiscent of the phenotype in naturally aged WT mice, in which there is a decrease in cell number, but all T-cell subsets are present and the proportions of T-cell subsets do not change [29, 30].

The defective thymus in nude-K14Cre-fx/fx mice produces a large number of morphologic pulmonary alveolar-like 2D-epithelial cysts

To determine whether the reduction in cellularity is the sole phenotype and what changes occur inside the thymus of nude-K14Cre-fx/fx mice, we investigated the thymic micro-architecture using immunohistological approaches. Interestingly, we found that K14-driven *FoxN1* deletion induced the formation of many morphologic pulmonary alveolar-like cystic cavities in the medulla of the thymus (Fig. 3A, middle and right panels), similar to the lung alveoli (Supplemental Fig. S4A). Moreover, these cysts expanded with age and spread throughout the whole thymus (Fig. 3B, middle and right panels). Although a few thymic cyst structures persist in the normal developing thymus, they form a minor component of the overall thymus [2,3]. The increase in thymic cyst numbers and size represent the disruption of an organized 3D-TEC meshwork [4,5]. Interestingly, the spotted distribution of thymic cysts in the medulla is reminiscent of the scenario in which the medullary compartment develops from islets of clonally-derived cells [31]. If the normal islets of progenitor cells are disrupted, the spot shape mutant phenotype should be formed.

The thymic cysts have been reported as 2D structures only in terms of their morphology [4,5], - whether they are polarized, which is a feature of 2D epithelial structure in the skin and lung (Supplemental Fig. S4B), is unknown. So we proceeded to determine whether the cysts exhibit polarization. Immunofluorescent staining was performed using antibodies against two types of epithelial markers: K5, which is a stellate shaped mTEC marker in the thymus, but a basal layer marker in the skin and lung; and K8, which is a cTEC marker in the thymus, but an apical marker in the skin and lung. Our results indicated that these cysts were located in the $K5^+$ concentrated medullary regions (Fig. 3C, right panel), and the cystic lining differentially expressed polarized keratin types in each sides. Characterically, K5 was

expressed in the side connected to thymic tissue, while K8 in the side towards the cavity (Fig. 3D), which is very similar to the airway epithelial model (Supplemental Fig. S4B) and lung epithelial stem cell differentiated 2D tracheospheres [32].

The cyst-lining epithelium is composed of immature or degenerated TECs instead of mature TECs

To delineate the role of FoxN1 in cyst formation, we wanted to know whether immature or mature mTECs are present in the cyst-lining epithelium of the medullary region. If the cysts are derived from mature mTECs, it implies that FoxN1 may be involved in preventing mature mTECs from progressive regression, whereas if the cysts are derived from immature epithelium, the mechanism of cyst formation may be due to a blockage in epithelial stem cell differentiation caused by a shortage of FoxN1. Using multiple combinations of immunofluorescent antibody staining, we found that the nude-K14Cre-fx/fx thymus had significantly reduced UEA-1 expression, which marks organized mature mTECs, and the cyst-lining itself did not express UEA-1 (Figs. 4A, B, and C). The cyst-lining epithelium also stained weakly for MHC-II^{+} (Figs. 4C and D), which can also be regarded as mature TEC maker because mature TECs, particular mature mTECs, have high MHC-II expression. In some cases, MHC-II – stained with green fluorescence was found to be expressed in the pre-cystic lining (an incomplete cycle of cyst, which showed co-stained yellow cystic lining, arrows in Fig. 4D), but the expression seemed to fade (arrowheads in Fig. 4D, showing red due to reduction of the green fluorescence intensity) when the cysts were completely formed. However, the cyst-lining epithelium very strongly expressed Claudin-3^{+}&-4^{+} (Cld3,4^{+}), which are markers of the presumptive mTEC precursors [6] (Figs. 4D and E). Taken together, the thymic cystic epithelium likely represents under-developed immature TEC progenitor cells.

Increased expression of Cld3,4 in the cyst-lining epithelium, similar to Cld3,4 expression in 2D airway epithelium (Supplemental Fig. S4C), implies that there is a switch from non-polarized 3D- to polarized 2D-epithelium, because Claudins, as tight junction-related structural proteins and hallmark structures of 2D sheet-like epithelium, function by keeping stratified squamous epithelial cells permeable and polarized [33].

Increased numbers of Cld3,4^{+} TECs in the nude-K14Cre-fx/fx mice did not promote greater production of Aire^{+} mTECs

The *Aire* (autoimmunity regulator) gene is known to be expressed in mature mTECs. It has been reported that the Cld3,4^{+} (CD45UEA-1^{lo}MHC-II$^{lo/-}$) TEC subset is the presumptive precursor of Aire^{+} mature mTECs in the normal thymus [6]. We found that Cld3,4 expression was enhanced in the cyst-lining epithelium (Figs. 4D and E) and the proportion of total Cld3,4^{+} TECs in CD45UEA-1^{lo} TSCs was increased (Fig. 5A) in the nude-K14Cre-fx/fx mice. To determine whether increased Cld3,4 expression in the nude-K14Cre-fx/fx mice enhances or hinders the generation of Aire^{+} mTECs, we observed *Aire* gene expression by RT-PCR and Aire^{+} TECs by immunohistology in the nude-K14Cre-fx/fx thymi. The results show that both Aire mRNA expression (Fig. 5B) and Aire^{+} TECs (Fig. 5C) were significantly reduced. Furthermore, we found that Aire^{+} TECs were not derived from the Cld3,4^{+} cyst-lining epithelium itself, because even the nude-K14Cre-fx/fx thymus had Aire^{+} TECs, they were not present in the cystic lining itself (Fig. 5C bottom left panel). This implies that enhanced Cld3,4 expression in the cyst-lining epithelium and the increase in the proportion of Cld3,4^{+} TECs in the absence of FoxN1 does not promote Aire^{+} mTEC generation. These results are in accordance with observations of other gene mutation-caused thymic cysts. For example, in the aly/aly mouse thymus, Aire^{+} TECs were decreased although the cyst-lining epithelium had a large accumulation of Cld3,4^{+} TECs [6].

Epithelial cysts in the nude-K14Cre-fx/fx mice increase in size and number with age

Because FoxN1$^+$ TECs decrease with age [34] and the nude-K14Cre-fx/fx mouse phenotypes are caused by continuous K14-ΔE5&6-deletion from embryonic fertilization to postnatal life, we believe that the formation of the 2D cysts is a dynamic process. Therefore, questions about when these epithelial cysts are formed and whether they are getting worse with age were raised. To address these questions, cysts in the thymus from 2-week-old to 5-month-old mice were observed. We found that overt cysts in the medulla were present in mice from the age of 1 month and had worsened by the age of 5 months with an increase in both cyst number and size (Fig. 6), as well as a decrease in UEA-1$^+$ mature mTECs (Fig. 6A) and an increased accumulation of Cld3,4$^+$ TECs in the cyst-lining epithelium (Fig. 6B). Therefore, the epithelial cysts phenotype worsened with age.

Discussion

The functional thymus is largely dependent on a 3D-oriented TEC-constituted micro-structure, for instance, 2D-monolayer non-manipulated (non-Notch ligand transformed) stromal cells can not support T-cell development in culture, while reaggregated stromal cell-constituted 3D pseudo-thymic lobes can fully support T-cell development. It was also reported that dissociated thymic stromal cells (2D) lost, while reaggregated thymic stromal cells (3D) regained the Notch ligand Delta-like expression [35], which is crucial for T-cell development. On the other hand, epithelial cells in the lung and skin are dependent on a 2D structure and basal-apical cell polarity. The formation of thymic cysts represents an alteration of the epithelial microstructure from 3D to 2D [4,5], and a thymic to pulmonary shift in morphological features [2]. Although a 2D epithelial structure is normal in the lung, it is abnormal in the thymus. Gene mutations can increase the generation of 2D-thymic cysts *in vivo*, while abnormal culture conditions, such as adding dGUO can induce their formation *in vitro*. In this study, we used a novel K14-ΔE5&6-deletion mouse model which results in a keratin type-specific FoxN1 mutation. The mutation caused by the K14-ΔE5&6-deletion is neither equivalent to a FoxN1-null mutation [17], nor to the FoxN1 partial/hypomorphic mutation [22]. By using this mutation we present three novel findings as follow. **First**, we demonstrated that loss of *FoxN1* exons-5 and -6 in K14 promoter-driven TECs induced an increase in the formation of 2D-thymic epithelial cysts that were specifically located in the medullary region, and the number of cysts increased with age. The 2D-thymic epithelial cystic lining clearly expressed polarized differential keratin types in each side. Although Cld3,4$^+$ TECs have been reported as precursors of Aire$^+$ mature mTECs [6], increased expression of Cld3,4 in the 2D-thymic epithelial cyst-lining did not induce the generation of more UEA-1$^+$ and Aire$^+$ mature mTECs. **Second**, we also established that FoxN1 in K14 epithelium has distinct impacts on epithelial cell development in the thymus and skin. The K14-specific *FoxN1* deletion was sufficient to induce a hair follicle defect that resulted in a nude phenotype, similar to that of the FoxN1-null mutant mice, but could not induce athymia, thus different from the thymic phenotype of the FoxN1-null mutant mice. **Third**, we solidified the fact that FoxN1 is required not only for prenatal but also for postnatal epithelial development, because deletion of *FoxN1* in prenatal (mediated by Cre-recombinase from parents) life alone cannot induce the above phenotypes.

The 2D-thymic cystic epithelial structure is evident not only in the sheet-like epithelial morphology, but also from changes in protein expression. The enhancement and accumulation of Cld3,4 expression are proof that the non-polarized 3D-epithelium changes to polarized 2D-epithelium, because increased expression of Claudins reflects an increase in permeability and polarity of stratified squamous epithelial cells [33]. Cld3,4$^+$ is also a marker of immature mTECs [6]. Based on the high levels of Cld3,4 expression and reduced MHC-II expression, the thymic cyst-lining epithelia should represent under-developed immature TECs instead of mature mTECs. However, when there is a shortage of FoxN1 in

the K14-ΔE5&6-deletion thymus, i.e., loss of *FoxN1* in K14 promoter-driven TECs, these immature cells seem to lose the potential to develop into UEA-1^+ and $Aire^+$ mature TECs, because both UEA-1^+ and $Aire^+$ mature mTECs have been found to be significantly decreased (Figs. 4A and 5C). Therefore, FoxN1 is involved in the morphogenesis and maintenance of 3D thymic microstructure and regulation of TEC maturation.

A recent report [36] showed that $FoxN1^+$ TECs are considered as TEC progenitors in both the pre- and post-natal thymus, while FoxN1-negative TECs in the postnatal thymus, which do not contribute to thymopoietic function are descendants of $FoxN1^+$ progenitors. This finding coincides with our point that deletion of *FoxN1* in epithelial cells causes disruption of epithelial progenitors which are functional to generation and maintenance of TEC homeostasis. $FoxN1^+$ K14 epithelial cells are possible one of epithelial progenitor subsets. Our report showed the distribution, morphology, and age at the time of formation of the thymic cysts provides insights into the role of FoxN1 in K14 promoter-driven TEC progenitors. Because the K14 promoter has the potential to be active in epithelial stem cells (22,23), the defect in the K14-ΔE5&6-deletion thymus may be due to a blockage in the differentiation of immature precursors into the mature mTECs. The K14-activity in TEC progenitors is likely to be present in many islets in the medulla of the adult thymus [31], because the defect generated alveolar-like or islet-like 2D-epithelial cysts in the medulla, but had little effect on cTECs. Although both K14 and K5 are expressed in the medulla and may be co-expressed in the cortico-medullary junction, and $K14^+$ and $K5^+$ TECs have very similar morphology (stellate shape), it is very likely that the K14 and K5 promoters are active in different TEC progenitors, because the thymic medulla has a heterogeneous population of mTECs, including at least $K5^+$, $K14^+$, UEA-1^+ mTEC subsets. This is also supported by the fact that *FoxN1* deletion in both keratin promoter-driven Cre/$CreER^T$ displayed different severities in thymocyte development [20]. Deleting *FoxN1* ΔE5&6 in K14 TECs in the embryo alone (solely parents' Cre) does not induce a phenotype in the adults (haired-fx/fx mice with K14Cre-ΔE5&6-deletion), whereas, a continuous deletion mediated by a self-Cre in postnatal life is required for generation of the phenotype in the adults. This implies that FoxN1-regulated epithelial stem cells exist and play an important role in the postnatal thymus. That is why resuming FoxN1 expression in the FoxN1 mutant postnatal thymus can re-generate the thymus in adulthood [37]. Although the K14-ΔE5&6-deletion is initiated in germ cells (activated Cre protein from parental oocytes and zygotes), the 2D-thymic epithelial cysts in the nude-K14Cre-fx/fx thymus were formed postnatally after 2 weeks of age. This could be due to a combination of two FoxN1-dependent mechanisms: i), A defect in morphogenesis: the deletion of *FoxN1* at the germline level causes developmental insufficiency of epithelial patterning at the second genetic step [17] of thymic organogenesis at the fetal stage. However, this mechanism alone cannot induce 2D-thymic cysts in the K14Cre-fx/fx mice as demonstrated by the haired-fx/fx mouse with K14-ΔE5&6-deletion (Fig. 1). Therefore, a second mechanism is required: ii), Failure in postnatal maintenance: the continuous deletion of *FoxN1* in the postnatal K14-expressing TECs results in an insufficient supply of continuously differentiated TECs. Therefore, the postnatal TEC homeostasis cannot be maintained. These mechanisms aggregately produce the thymic cystic phenotypes. This finding also coincides with and further confirms our previous report that FoxN1 has an age-associated requirement in the thymus [34].

Observations of FoxN1 expression and function in the skin and thymus have shown that on addition to the common role of FoxN1 in regulating skin and thymic epithelial cell differentiation, it has different roles/impacts in the skin and thymus. For example, FoxN1 regulates the morphogenesis and maintenance of 3D-TEC micro-structure in the thymus, but also maintains 2D-epithelial micro-structure in the skin (Details listed in Supplemental Table S2). Moreover, the K14-ΔE5&6-deletion mediated by both parents and self K14Cre during and after fertilization is sufficient to induce a hairless phenotype in the skin, and

produces an effect similar to that in the *FoxN1*-null nude mouse, but is not sufficient to induce athymia, thus, differing from the effect in the *FoxN1*-null nude mouse thymus. Our data demonstrate that the previously accepted concept that the thymus is more sensitive than the skin to the loss of FoxN1 is not always the case. Deletion of *FoxN1* exons-5&6 in K14 positive epithelial cells only causes the nude skin phenotype but not the athymic phenotype. This may account for the K14 promoter-driven epithelial stem cells exhibiting distinctive activity in the skin and thymus. The K14 promoter is expressed and exhibits activity in the skin and mammary gland epithelial progenitors in the basal layer, and these cells are able to give rise to both basal and luminal lineages [15, 16]. In the thymus, the K14 promoter likely exhibits activity in thymic epithelial progenitors that may be restricted to the medulla with an islet distribution. As for differences in FoxN1 expression in the skin and thymus, it is relatively restricted to the hair cortex in the skin and functions primarily to regulate the development and pigmentation of the hair cortex. In the thymus, FoxN1 is expressed in both the cortex and medulla, particularly in medullary epithelial subset, and functions primarily to maintain the steady-state medulla in the postnatal thymus [20]. It appears that the cortical and medullary epithelia in the hair follicle and in the thymus are of varying importance in postnatal mice. The cortical epithelium in the postnatal hair follicle is important for preventing nude skin, while the medullary epithelium in the postnatal thymus is important for preventing thymic atrophy [20]. Therefore, we suggest that FoxN1 in K14 promoter-driven epithelial progenitors might play a dominant role in the skin, while it is not dominant in the thymus.

The highly cystic thymic microenvironment associated with a decrease in medullary $Aire^+$ mTECs results in an inability to promote and maintain proper T-lymphocyte development in the medulla, which is the primary site for the generation of central immune tolerance. This damage in the nude-K14Cre-fx/fx mice may cause “holes” in the TCR repertoire diversity and make the mice more prone to autoimmunity. Although we have not directly found obvious spontaneous autoimmune diseases caused by this defect, we observed an autoimmune-prone. By using a low dose of influenza virus infection can cause severe immunopathological changes in these mice, although they have a decreased CD8 specific T-cell reaction (our unpublished data). This was also demonstrated by other immune deficient and autoimmune mouse models, such as ALY (severe immunodeficiency) and NOD (insulin-dependent diabetes) mice. Their thymi also exhibit an increase in irregular cystic cavities. In summary, FoxN1 is confirmed to be involved in the maintenance of the 3D-thymic epithelial structure, potentially through the regulation of postnatal epithelial stem cell differentiation. Therefore, this study raises a number of important issues regarding gene regulation in the morphogenesis and maintenance of thymic epithelial 3D-microstructure and mechanisms of central immune tolerance.

Supplementary Material

Refer to Web version on PubMed Central for supplementary material.

Acknowledgments

We thank Dr. **Janice L. Brissette** (Massachusetts General Hospital and Harvard Medical School) for providing insightful discussion about skin phenotype and Cre transgenic mouse mating strategies, Dr. **Takashi Amagai** (Meiji University of Integrative Medicine, Kyoto, Japan) for providing FoxN1 antibody, Dr. **Ramesh Nayak** (UTHSCT) for confocal microscopy, and **Sandra E. Nash** (UTHSCT) for cryo-sectioning work.

Funding support: This work was supported by the NIAID/NIH grants (R01AI081995 and R21AI079747) to D-M S.

Abbreviations

Aire	autoimmune regulator gene
cTEC/mTEC	cortical/medullary thymic epithelial cells
fx	*loxP*-floxed-*FoxN1*
K14Cre	Keratin-14 promoter-driven Cre-recombinase
LPC	lympho-hematopoietic progenitor cells
Tg	transgene
TSC	thymic stromal cell
WT	wild type

References

1. van Ewijk W, Wang B, Hollander G, Kawamoto H, Spanopoulou E, Itoi M, Amagai T, Jiang YF, Germeraad WT, Chen WF, Katsura Y. Thymic microenvironments, 3-D versus 2-D? Semin Immunol. 1999; 11:57–64. [PubMed: 9950752]
2. Dooley J, Erickson M, Farr AG. An organized medullary epithelial structure in the normal thymus expresses molecules of respiratory epithelium and resembles the epithelial thymic rudiment of nude mice. J Immunol. 2005; 175:4331–4337. [PubMed: 16177073]
3. Farr AG, Dooley JL, Erickson M. Organization of thymic medullary epithelial heterogeneity: implications for mechanisms of epithelial differentiation. Immunol Rev. 2002; 189:20–27. [PubMed: 12445262]
4. Vroegindeweij E, Crobach S, Itoi M, Satoh R, Zuklys S, Happe C, Germeraad WT, Cornelissen JJ, Cupedo T, Hollander GA, Kawamoto H, van Ewijk W. Thymic cysts originate from Foxn1 positive thymic medullary epithelium. Mol Immunol. 2010; 47:1106–1113. DOI S0161-5890(09)00807-4 [pii] 10.1016/j.molimm.2009.10.034. [PubMed: 19945167]
5. Germeraad WT, Kawamoto H, Itoi M, Jiang Y, Amagai T, Katsura Y, van Ewijk W. Development of thymic microenvironments in vitro is oxygen-dependent and requires permanent presence of T-cell progenitors. J Histochem Cytochem. 2003; 51:1225–1235. [PubMed: 12923248]
6. Hamazaki Y, Fujita H, Kobayashi T, Choi Y, Scott HS, Matsumoto M, Minato N. Medullary thymic epithelial cells expressing Aire represent a unique lineage derived from cells expressing claudin. Nat Immunol. 2007; 8:304–311. [PubMed: 17277780]
7. Anderson G, Lane PJ, Jenkinson EJ. Generating intrathymic microenvironments to establish T-cell tolerance. Nat Rev Immunol. 2007; 7:954–963. DOI nri2187 [pii] 10.1038/nri2187. [PubMed: 17992179]
8. Anderson G, Owen JJ, Moore NC, Jenkinson EJ. Thymic epithelial cells provide unique signals for positive selection of CD4+CD8+ thymocytes in vitro. J Exp Med. 1994; 179:2027–2031. [PubMed: 7910843]
9. Koble C, Kyewski B. The thymic medulla: a unique microenvironment for intercellular self-antigen transfer. J Exp Med. 2009; 206:1505–1513. DOI jem.20082449 [pii] 10.1084/jem.20082449. [PubMed: 19564355]
10. Villasenor J, Benoist C, Mathis D. AIRE and APECED: molecular insights into an autoimmune disease. Immunol Rev. 2005; 204:156–164. [PubMed: 15790357]
11. Fontenot JD, Dooley JL, Farr AG, Rudensky AY. Developmental regulation of Foxp3 expression during ontogeny. J Exp Med. 2005; 202:901–906. [PubMed: 16203863]
12. Gallegos AM, Bevan MJ. Central tolerance: good but imperfect. Immunol Rev. 2006; 209:290–296. [PubMed: 16448550]
13. Klug DB, Carter C, Crouch E, Roop D, Conti CJ, Richie ER. Interdependence of cortical thymic epithelial cell differentiation and T-lineage commitment. Proc Natl Acad Sci U S A. 1998; 95:11822–11827. [PubMed: 9751749]

14. Klug DB, Carter C, Gimenez-Conti IB, Richie ER. Cutting edge: thymocyte-independent and thymocyte-dependent phases of epithelial patterning in the fetal thymus. J Immunol. 2002; 169:2842–2845. [PubMed: 12218095]
15. Vassar R, Rosenberg M, Ross S, Tyner A, Fuchs E. Tissue-specific and differentiation-specific expression of a human K14 keratin gene in transgenic mice. Proc Natl Acad Sci U S A. 1989; 86:1563–1567. [PubMed: 2466292]
16. Kuraguchi M, Ohene-Baah NY, Sonkin D, Bronson RT, Kucherlapati R. Genetic mechanisms in Apc-mediated mammary tumorigenesis. PLoS Genet. 2009; 5:e1000367. DOI 10.1371/journal.pgen.1000367. [PubMed: 19197353]
17. Nehls M, Kyewski B, Messerle M, Waldschutz R, Schuddekopf K, Smith AJ, Boehm T. Two genetically separable steps in the differentiation of thymic epithelium. Science. 1996; 272:886–889. [PubMed: 8629026]
18. Nehls M, Pfeifer D, Schorpp M, Hedrich H, Boehm T. New member of the winged-helix protein family disrupted in mouse and rat nude mutations. Nature. 1994; 372:103–107. [PubMed: 7969402]
19. Cunningham-Rundles C, Ponda PP. Molecular defects in T- and B-cell primary immunodeficiency diseases. Nat Rev Immunol. 2005; 5:880–892. [PubMed: 16261175]
20. Cheng L, Guo J, Sun L, Fu J, Barnes PF, Metzger D, Chambon P, Oshima RG, Amagai T, Su DM. Postnatal tissue-specific disruption of transcription factor FoxN1 triggers acute thymic atrophy. J Biol Chem. 2010; 285:5836–5847. DOI M109.072124 [pii] 10.1074/jbc.M109.072124. [PubMed: 19955175]
21. Dassule HR, Lewis P, Bei M, Maas R, McMahon AP. Sonic hedgehog regulates growth and morphogenesis of the tooth. Development. 2000; 127:4775–4785. [PubMed: 11044393]
22. Su DM, Navarre S, Oh WJ, Condie BG, Manley NR. A domain of Foxn1 required for crosstalk-dependent thymic epithelial cell differentiation. Nat Immunol. 2003; 4:1128–1135. [PubMed: 14528302]
23. Dooley J, Erickson M, Farr AG. Alterations of the medullary epithelial compartment in the Aire-deficient thymus: implications for programs of thymic epithelial differentiation. J Immunol. 2008; 181:5225–5232. DOI 181/8/5225 [pii]. [PubMed: 18832676]
24. Gui J, Zhu X, Dohkan J, Cheng L, Barnes PF, Su DM. The aged thymus shows normal recruitment of lymphohematopoietic progenitors but has defects in thymic epithelial cells. Int Immunol. 2007; 19:1201–1211. DOI dxm095 [pii] 10.1093/intimm/dxm095. [PubMed: 17804689]
25. Hafner M, Wenk J, Nenci A, Pasparakis M, Scharffetter-Kochanek K, Smyth N, Peters T, Kess D, Holtkotter O, Shephard P, Kudlow JE, Smola H, Haase I, Schippers A, Krieg T, Muller W. Keratin 14 Cre transgenic mice authenticate keratin 14 as an oocyte-expressed protein. Genesis. 2004; 38:176–181. DOI 10.1002/gene.20016. [PubMed: 15083518]
26. Ramirez A, Page A, Gandarillas A, Zanet J, Pibre S, Vidal M, Tusell L, Genesca A, Whitaker DA, Melton DW, Jorcano JL. A keratin K5Cre transgenic line appropriate for tissue-specific or generalized Cre-mediated recombination. Genesis. 2004; 39:52–57. DOI 10.1002/gene.20025. [PubMed: 15124227]
27. Brissette JL, Li J, Kamimura J, Lee D, Dotto GP. The product of the mouse nude locus, Whn, regulates the balance between epithelial cell growth and differentiation. Genes Dev. 1996; 10:2212–2221. [PubMed: 8804315]
28. Lee D, Prowse DM, Brissette JL. Association between mouse nude gene expression and the initiation of epithelial terminal differentiation. Dev Biol. 1999; 208:362–374. [PubMed: 10191051]
29. Thoman ML. The pattern of T lymphocyte differentiation is altered during thymic involution. Mech Ageing Dev. 1995; 82:155–170. [PubMed: 8538244]
30. Aspinall R. Age-associated thymic atrophy in the mouse is due to a deficiency affecting rearrangement of the TCR during intrathymic T cell development. J Immunol. 1997; 158:3037–3045. [PubMed: 9120255]
31. Rodewald HR, Paul S, Haller C, Bluethmann H, Blum C. Thymus medulla consisting of epithelial islets each derived from a single progenitor. Nature. 2001; 414:763–768. [PubMed: 11742403]

32. Rock JR, Onaitis MW, Rawlins EL, Lu Y, Clark CP, Xue Y, Randell SH, Hogan BL. Basal cells as stem cells of the mouse trachea and human airway epithelium. Proc Natl Acad Sci U S A. 2009; 106:12771–12775. DOI 0906850106 [pii] 10.1073/pnas.0906850106. [PubMed: 19625615]

33. Lal-Nag M, Morin PJ. The claudins. Genome Biol. 2009; 10:235. DOI gb-2009-10-8-235 [pii] 10.1186/gb-2009-10-8-235. [PubMed: 19706201]

34. Sun L, Guo J, Brown R, Amagai T, Zhao Y, Su DM. Declining expression of a single epithelial cell-autonomous gene accelerates age-related thymic involution. Aging Cell. 2010; 9:347–357. DOI ACE559 [pii] 10.1111/j.1474-9726.2010.00559.x. [PubMed: 20156205]

35. Mohtashami M, Zuniga-Pflucker JC. Three-dimensional architecture of the thymus is required to maintain delta-like expression necessary for inducing T cell development. J Immunol. 2006; 176:730–734. [PubMed: 16393955]

36. Corbeaux T, Hess I, Swann JB, Kanzler B, Haas-Assenbaum A, Boehm T. Thymopoiesis in mice depends on a Foxn1-positive thymic epithelial cell lineage. Proc Natl Acad Sci U S A. 2010 DOI 1004623107 [pii] 10.1073/pnas.1004623107.

37. Bleul CC, Corbeaux T, Reuter A, Fisch P, Monting JS, Boehm T. Formation of a functional thymus initiated by a postnatal epithelial progenitor cell. Nature. 2006; 441:992–996. [PubMed: 16791198]

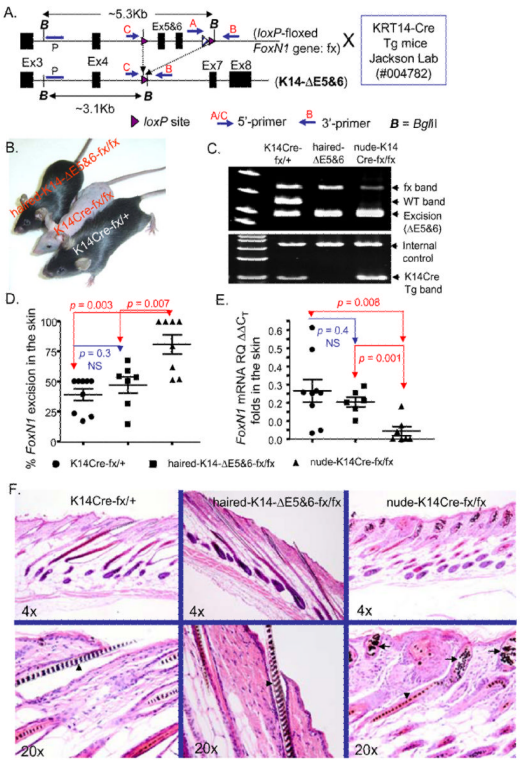

Figure 1. Keratin-14Cre mediated *FoxN1* ΔE5&6-deletion generates nude K14Cre-fx/fx homozygous mice

(A) A schematic of *loxP*-floxed *FoxN1* mice crossed (denoted by an enlarged "X" in panel A) with K14Cre transgenic mice, before (top) and after (bottom) *FoxN1* ΔE5&6-excision (i.e., K14 promoter-driven Cre-mediated deletion of exons 5 and 6 of *FoxN1* locus). **(B)** Gross appearance of haired-fx/fx mice with the K14-ΔE5&6-deletion, nude-K14Cre-fx/fx, and K14Cre-fx/+ mice (from left to right). **(C)** Top panel: representative results of a three-primer PCR (see Material and Methods and Supplemental Table S1) on skin genomic DNA of K14Cre-fx/+, haired-fx/fx with K14-ΔE5&6-deletion, and nude-K14Cre-fx/fx (from left to right) mice. Bottom panel: representative results of a K14Cre PCR with internal control (see Supplemental Table S1). **(D)** Summarized results show the incidence of the K14Cre-ΔE5&6-deletion at genomic DNA level in the skin analyzed by three-primer PCR from three genotypic mice. The % K14Cre-ΔE5&6-deletion was calculated as the % of the signal from the excision band / (excision band + fx band) in fx/fx homozygotes, or the excision band / ½ (excision band + fx band + WT band) in fx/+ heterozygotes. **(E)** Summarized results show changes in relative folds of FoxN1 mRNA in the skin of mice of the three genotypes analyzed by real-time RT-PCR from. In D and E, each circle, square, and triangle represents data from one animal. **(F)** A representative H&E staining of the skin hair follicles of K14Cre-fx/+ (left panels), haired-fx/fx with K14Cre-mediated *FoxN1* deletion (middle panels), and nude-K14Cre-fx/fx (right panels) mice, respectively. The arrowheads in the lower panels indicate the cortex of the hair follicles. The arrows in the lower right panel show the degraded hair follicles.

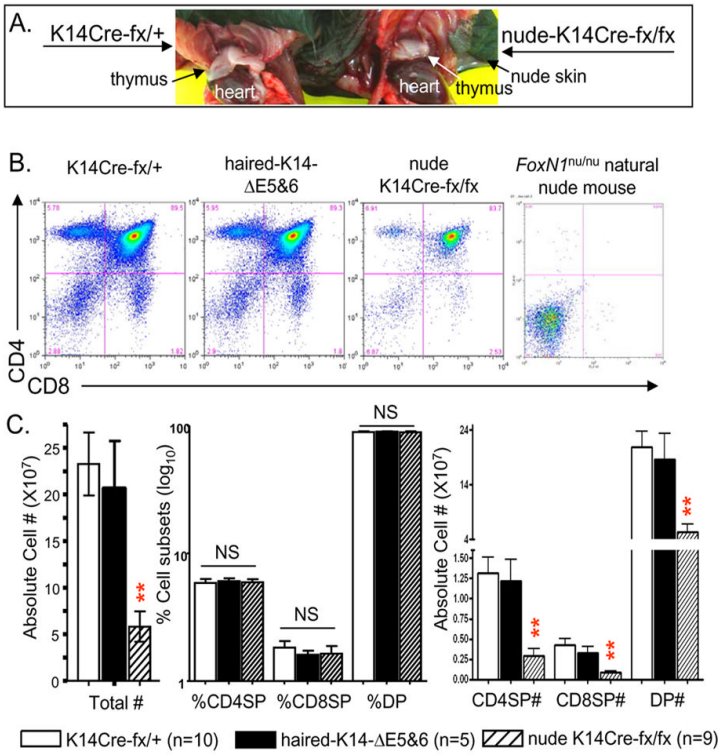

Figure 2. K14 promoter-driven *FoxN1* ΔE5&6-deletion causes defects in thymocyte development

(A) A gross view of thymic size in K14Cre-fx/+ (left) and nude-K14Cre-fx/fx (right) mice. An un-cropped image of these mice is shown in Supplemental Fig. S2. **(B)** A representative result from a FACS profile of CD4 vs. CD8 thymocytes from mice of four different genotypes. **(C)** The summarized results of the total thymic cell numbers (left panel), percentages of CD4SP, CD8SP and DP thymocytes (middle panel), as well as absolute cell numbers per thymus of CD4SP, CD8SP and DP thymocytes (right panel) from mice of three different genotypes. ** = very significant difference ($p < 0.01$) between nude-14Cre-fx/fx mice (striped bars) and either K14Cre-fx/+ mice (empty bars) or haired-fx/fx mice with K14Cre-ΔE5&6-deletion (dark bars).

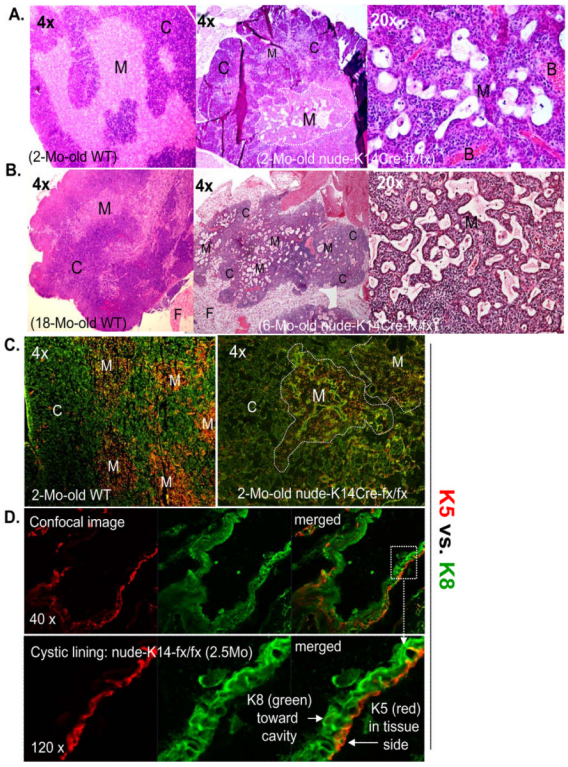

Figure 3. K14Cre-mediated *FoxN1* ΔE5&6-deletion induces morphologic pulmonary alveolar-like 2D-epithelial cysts in the thymus

(A) and **(B)** A representative result of H&E staining is shown for at least two experiments, with essentially identical results. Left panels show thymic cortex "C" and medulla "M" from 2-month-old (A) and 18-month-old (B) WT mice at 4× magnification. Middle and right panels show morphologic pulmonary alveolar-like 2D-thymic cystic cavities in the medulla of 2-month-old (A) and 6-month-old (B) nude-K14Cre-fx/fx mice at 4× and 20× magnifications. F = fat tissue, B = blood vessels. **(C) and (D)** A representative immunofluorescent staining of K8 (green) and K5 (red) antibodies on cryosections, (C) at 4× magnification from ~2-month-old WT (left panel) and 2-month-old nude-K14Cre-fx/fx mouse thymi (right panels); (D) confocal images at 40× and 120× magnifications showing cystic lining from 2.5-month-old nude-K14Cre-fx/fx mouse. This experiment was done in at least 2 biological replicates, with essentially identical results. M = medulla, C = cortex.

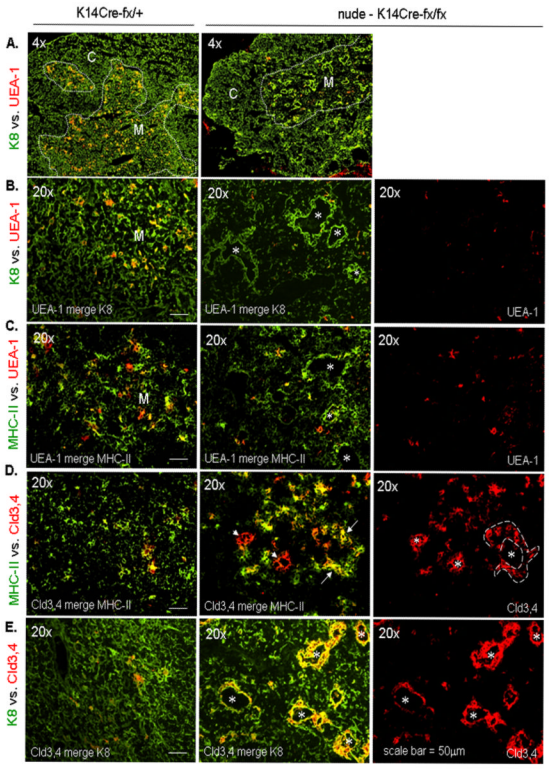

Figure 4. Immunofluorescent profiles of thymic cystic epithelial lining in the K14Cre-mediated *FoxN1* ΔE5&6 deleted thymus

All thymi were from ~2-month-old mice. **(A)** A representative immunofluorescent staining of K8 (green) and UEA-1 (red) antibodies on cryosections from K14Cre-fx/+ (left panel) and nude-K14Cre-fx/fx (right panel) thymi at 4× magnification. M = medulla, C = cortex, dashed lines = cortico-medullary junction. **(B-E)** A representative immunofluorescent staining of cryosections from K14Cre-fx/+ (left panels) and nude-K14Cre-fx/fx (middle and right panels) thymi at 20× magnification showing K8 (green) and UEA-1 (red) (B); MHC-II (green) and UEA-1 (red) (C); MHC-II (green) and Cld3,4 (red) (D); and K8 (green) and Cld3,4 (red) (E). All asterisks indicate thymic cystic cavities. Arrows in (D) show pre-cystic epithelial lining with equal MHC-II vs. Cld3,4 levels (yellow), arrowheads in (D) show cystic epithelial lining with reduced MHC-II expression (red). This experiment was done in 2~3 biological replicates, with essentially identical results.

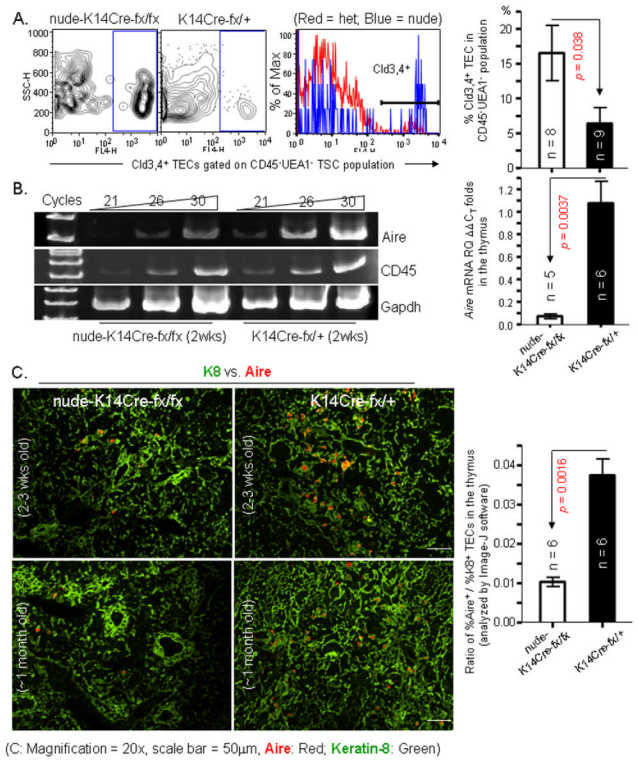

Figure 5. K14Cre-mediated *FoxN1* deletion causes an increase in the proportion of Cld3,4$^+$ TECs, but it does not enhance generation of Aire$^+$ mature mTECs

(A) Flow cytometric results show an increase in the proportion of Cld3,4$^+$ TECs in the CD45UEA-1$^-$ TSCs of the nude-K14Cre-fx/fx mice compared to K14Cre-fx/+ littermates. Left panels are representative flow cytometric profiles. Right bar graph is a summary of the results. **(B)** Left panel shows the decrease in Aire mRNA expression in TSC-enriched thymic cells [24] of the nude-K14Cre-fx/fx young (2-3 weeks old) mice compared to K14Cre-fx/+ littermates by a semi-quantitative RT-PCR. Right bar graph shows summarized results of changes in relative fold of Aire mRNA analyzed by real-time RT-PCR from the TSC-enriched thymic cells of the nude-K14Cre-fx/fx young (2-3 weeks old) mice and K14Cre-fx/+ littermates. **(C)** Images on the left show a representative merged immunofluorescent staining of K8 (green) and Aire (red) antibodies on cryosections from nude-K14Cre-fx/fx (top left panel: 2-3 weeks old and bottom left panel: ~1 month old) and K14Cre-fx/+ (top right panel: 2-3 weeks old and bottom right panel: ~1 month old) mouse thymi. Right bar graph shows summarized ratio of % Aire$^+$ areas versus % K8$^+$ regions analyzed by NIH software image-J.

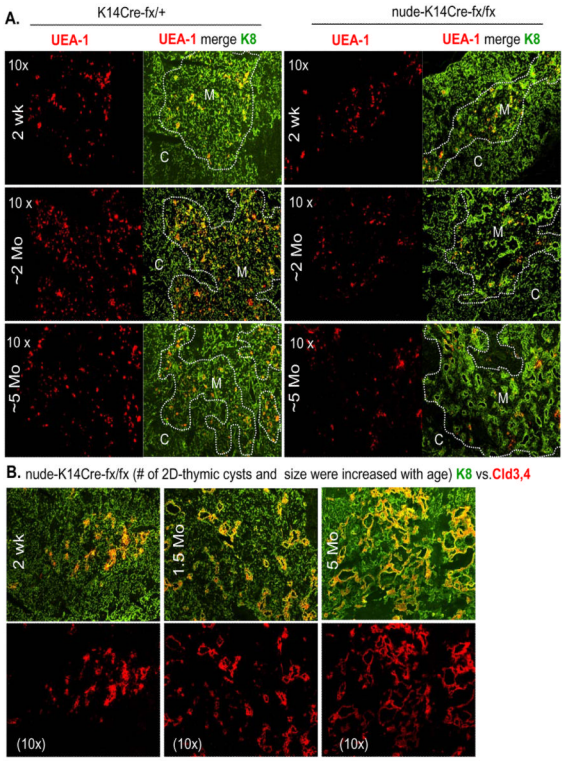

Figure 6. Age-associated increase in thymic cystic cavities in nude-K14Cre-fx/fx mice

(A) A representative immunofluorescent staining of K8 (green) and UEA-1 (red) antibodies on cryosections from K14Cre-fx/+ (left two panels) and nude-K14Cre-fx/fx (right two panels) mouse thymi at the age of 2 weeks (top panels), ~2 months (middle panels), and ~5 months (bottom panels). The left panels in each sample show UEA-1^{+} TECs, while the right panels in each sample show merged UEA-1^{+} and K8^{+} TECs. Dashed lines represent the cortico-medullary junction. M = medulla, C = cortex. **(B)** A representative merged immunofluorescent staining of K8 (green) and Cld3,4 (red) antibodies on cryosections from nude-K14Cre-fx/fx mouse thymi at the age of 2 weeks (left panels), ~2 months (middle panels), and ~5 months (right panels). These experiments were done in 2-3 biological replicates in per group, with essentially identical results.

Table 1

Haired/nude K14Cre-fx/fx mice derived from alternate mating strategies

Mating strategies			fx/fx pups with K14-ΔE5&6-deletion			
			haired		nude	
♂ (father)	♀ (mother)	Total fx/fx pups #	K14Cre^{+} (%)	K14Cre^{-} (%)	K14Cre^{+} (%)	K14Cre^{-} (%)
K14Cre^{+}-fx/fx (nude ♂)	fx/fx-only	17	0 (0%)	1 (5.9%)	6 (35.3%)	0 (0%)
fx/fx-only	K14Cre^{+}-fx/+	12	0 (0%)	5 (41.7%)	4 (33.3%)	0 (0%)

Note: Randomly chosen 6 litters. Pie graph is shown in supplemental Fig. S1.